

# Polarization Properties of Amorphous Chalcogenide Films with Laser-induced Periodic Structures

A. I. Musorin<sup>a,b,\*</sup>, D. I. Archibasov<sup>b</sup>, D. V. Shuleiko<sup>b</sup>, S. A. Kozyukhin<sup>c</sup>,  
P. K. Kashkarov<sup>b,d</sup>, and A. A. Fedyanin<sup>b</sup>

<sup>a</sup> Shenzhen MSU-BIT University, Shenzhen, 517182 P.R.C.

<sup>b</sup> Physical Department, Lomonosov Moscow State University, Moscow, 119991 Russia

<sup>c</sup> Kurnakov Institute of General and Inorganic Chemistry, Russian Academy of Sciences, Moscow, 119991 Russia

<sup>d</sup> National Research Center “Kurchatov Institute,” Moscow, 123182 Russia

\*e-mail: musorin@nanolab.phys.msu.ru

Received November 5, 2025; revised November 5, 2025; accepted November 18, 2025

**Abstract**—The need to replace bulk classical optical elements with their compact nanoscale counterparts stimulates research of new materials, their production and processing methods, optical properties calculation, and experimental verification. The possibility of using laser-induced periodic structures on the surface of thin chalcogenide As<sub>50</sub>Se<sub>50</sub> films as polarization optics elements has been studied. Designing the surface relief allows one to create waveplates with predetermined electromagnetic properties.

DOI: 10.1134/S2635167625601901

## INTRODUCTION

The polarization control is a key element for managing light parameters. Polarizing optical elements are important components of experimental scientific setups. Polarization control is also used in applied photonics. Wave plates and compensators play an important role in addition to polarizers. They delay one component of the electric field relative to another. In geometric optics, this is achieved using bulky anisotropic crystals, where an optical path difference  $\Delta x$  is proportional to the difference in the refractive indices of the ordinary and extraordinary waves  $\Delta n$ , as well as the material thickness  $d$ :  $\Delta x = \Delta n d$  [1]. Typically,  $\Delta n$  has a small value ( $10^{-2}$ – $10^{-3}$ ), leading to a large optical element thickness  $d$ . As anisotropic crystals are chosen quartz, various micas, and plastics. These materials limit the optical range of the resulting device, as well as its miniaturization potential.

To solve this problem, nanostructured elements with optical resonances have been proposed [2]. The electric field response of a light wave interacted with them differs for two components with mutually orthogonal polarizations due to the asymmetric shape of the nanoparticles. One of such examples is metasurfaces [3]. The fabrication of such nanostructures requires the use of electron lithography and etching, which limits the possibility of mass production and application of such devices, although, gives successful operation results.

An alternative approach for nanostructures manufacturing is direct laser writing, including application of ultrashort laser pulses [4]. This includes a wide range of methods, such as, for example, pulse laser deposition, where the material is changed due to its laser-induced melting or ablation caused by the absorption of high-power laser radiation [5]; or two-photon laser polymerization, which utilizes nonlinear optical effects in a photopolymer [6]. However, such methods usually do not allow achieving typical dimensions of the manufactured structures below a few micrometers.

Femtosecond laser action appears to be a promising tool for creating submicron elements using direct laser writing methods [7, 8], when the generation of laser-induced periodic surface structures (LIPSS) is observed with the typical size comparable to or smaller than the wavelength of the laser radiation [9].

LIPSS are formed due to the existence of a standing electromagnetic wave on the irradiated surface during the interaction of a high-power femtosecond laser pulse with the material [7–10]. If the energy absorbed in the antinodes of the standing wave exceeds the ablation threshold, a change in the material profile occurs, forming a periodic relief with a wave period [10]. When such one-dimensional grating is present on a surface of an optical device, it leads to different light behavior with polarization along and across the direction of the grating periodicity. A delay between these waves occurs, and, consequently, such structure acts as an analogue of a wave plate [11].

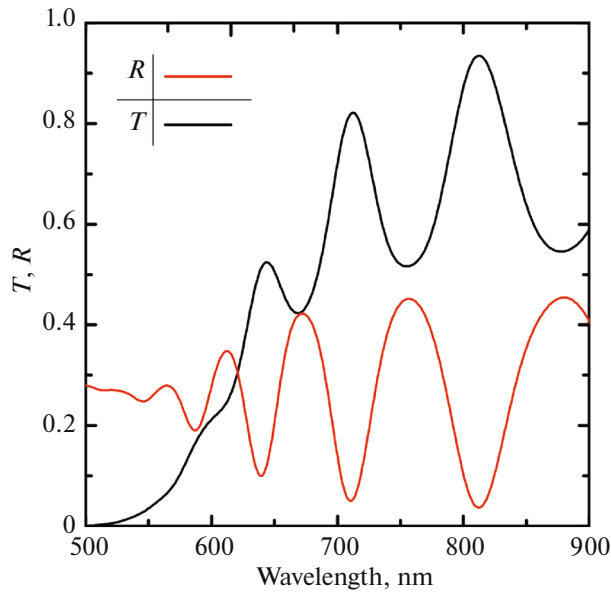


**Fig. 1.** Transmission and reflection spectra of the  $\text{As}_{50}\text{Se}_{50}$  film with a thickness of 885 nm. Black: transmission, red: reflection.

The LIPSS direct laser writing advantages are: the possibility of producing integrated optical elements by applying an optically anisotropic grating directly to the surface of another optical element (lens, mirror, fiber); free choice of the material, as it is known that LIPSS can be formed on metals [10, 12], semiconductors [10], including amorphous ones [7, 13, 14] and dielectrics [10, 15]; the possibility of adjusting the delay properties by controlling the formed relief through variation of the laser wavelength, power or repetition rate. These facts allow making wave plates with any delay.

In this work, we consider the formation of LIPSS in chalcogenide glasses based on arsenic selenide with the composition  $\text{As}_{50}\text{Se}_{50}$  [16]. As–Se systems exhibit high optical nonlinearity, the value of the third-order susceptibility is approximately 2 orders of magnitude higher than that of quartz glass [17], they are sensitive to the absorption of electromagnetic radiation and demonstrate various photoinduced effects under the influence of light. For example, they are used for ultra-fast switching in telecommunication systems [18]. The structure of the crystalline phase of  $\text{As}_{50}\text{Se}_{50}$  is similar to  $\alpha$ -realgar. The choice of the  $\text{As}_{50}\text{Se}_{50}$  compound is dictated by a lower melting temperature  $T_m = 550$  K relative to the analogous parameter for the  $\text{As}_{40}\text{Se}_{60}$  compound with  $T_m = 648$  K and which is widely used as a model chalcogenide glassy semiconductor [19]. It was assumed that the formation of

LIPSS in such a material is more probable and achievable under the applied irradiation parameters [20].

Thus, the aim of this work is to study the anisotropy of the optical properties of nanogratings formed by laser ablation on the surface of thin films from  $\text{As}_{50}\text{Se}_{50}$  chalcogenide glasses and to demonstrate the possibility of using them as wave plates and compensators.

## NUMERICAL CALCULATIONS

The calculations are realized using the finite-difference time-domain method. The calculation is carried out for one-dimensional gratings; therefore, a two-dimensional model is constructed under the assumption that the structure along the third axis is infinite. The  $Y$  axis is chosen as the direction of light propagation, and the  $X$  axis as the periodicity direction. Perfectly matched layers are set as the boundary conditions along the first axis, and periodic boundary conditions along the second one. Quartz is chosen as the substrate material with the fixed refractive index of 1.45. An 885-nm-thick  $\text{As}_{50}\text{Se}_{50}$  chalcogenide amorphous film is placed on top of the substrate. The real and imaginary parts of the refractive index of the film are taken from the literature [21]. A plane wave with a broad spectrum from 500 to 900 nm is taken as the radiation source, with two types of polarization: along the periodicity direction, i.e. codirectional with the wave vector of the surface grating (along the  $X$ , TM axis), and across it, along the grating grooves (along the  $Z$ , TE axis). Transmission and reflection spectra are studied for normal radiation incidence. Optical delay is studied using  $S$ -matrices, which describe transmission and reflection coefficients not by intensity, but by the field. The phase difference for the two polarizations yields the delay, which can be expressed in nanometers or wavelength units.

## RESULTS

At first, the unmodulated surface of the  $\text{As}_{50}\text{Se}_{50}$  thin film is studied. The transmission and reflection spectra are given in Fig. 1. Oscillations in the spectra are caused by interference in the thin film. The theoretical estimate of the interference period gives the value of 102 nm using the formula

$$\Delta\lambda = \frac{\lambda^2}{2dn}$$

Here, the wavelength  $\lambda$  is taken near 713 nm to be the position of the maximum,  $d = 885$  nm is the film thickness and  $n = 2.82$  is the refractive index. The results of simulation yield a value of  $\Delta\lambda = 102$  nm as well, defined as the difference between the maxima at 813 and 711 nm in the transmission spectrum.

Next, the surface of the  $\text{As}_{50}\text{Se}_{50}$  chalcogenide glass film is modulated using LIPSS. A cosine profile is assumed according to the formula

$$y(x) = y_0 + A \left( 1 + \cos \left( \frac{2\pi x}{P} \right) \right).$$

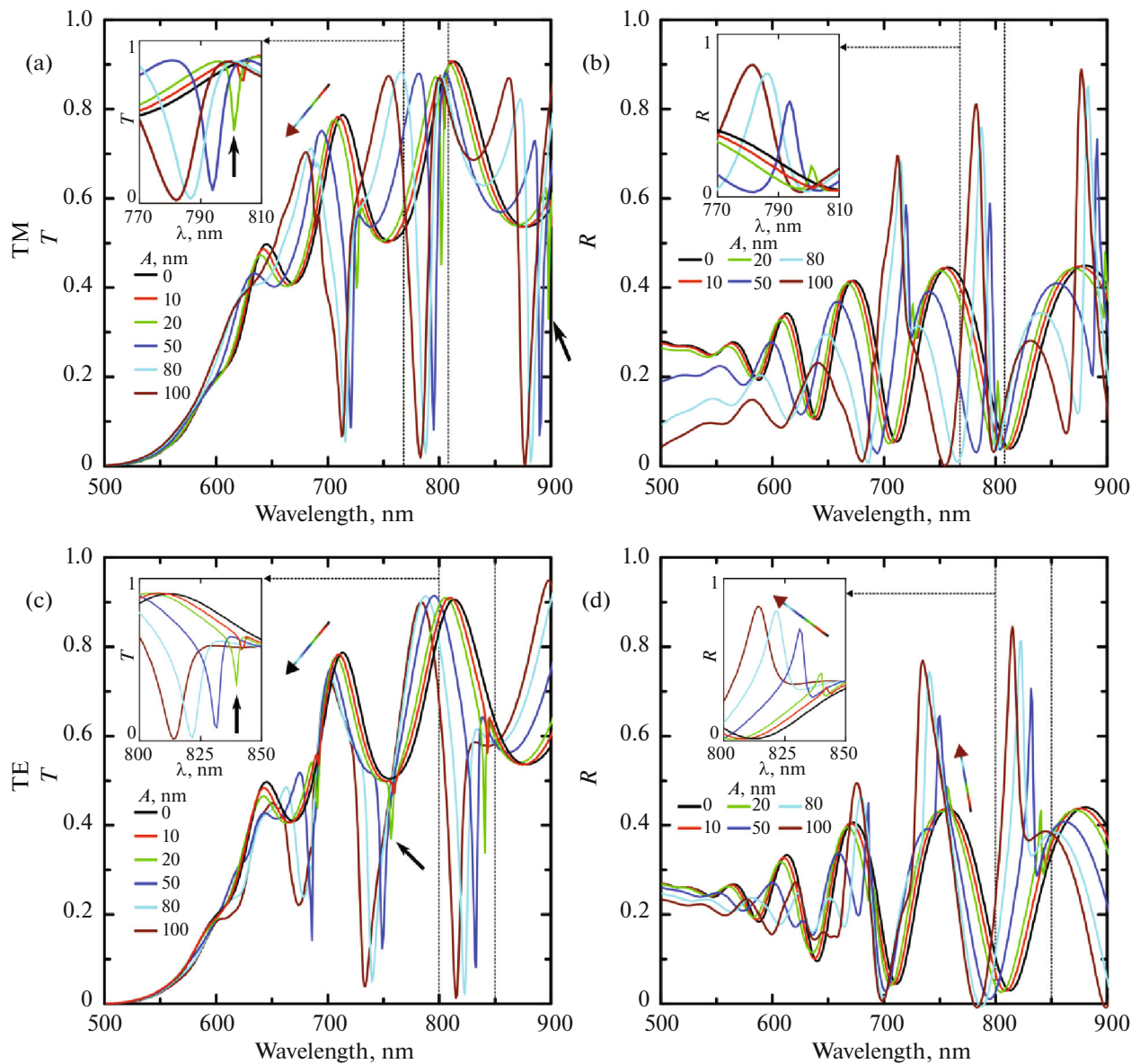
Here  $y_0$  is the thickness of the unmodulated layer,  $P$  is the grating period, and  $A$  is the surface modulation amplitude. The structure is periodic along the  $X$ -axis; its period is fixed at 472 nm. The amplitude is varied from 10 to 100 nm in 10 nm increment (for clarity, not all values will be presented below). The depth of the modulated layer is set in such a way that a thickness of the unstructured film  $y(x_0) = 885$  nm is achieved at maximum of the cosine function  $y(x_0)$ . This approach reproduces the patterning mechanism during LIPSS fabrication, when the surface relief is formed due to ablation of the film material [9]. The transmission and reflection spectra are calculated for the TE and TM polarizations of incident light for each type of surface morphology (Fig. 2). It should be mentioned that LIPSS can be understood in terms of a diffraction grating on the surface of a parallel-sided plate with thickness of  $(d - A)$  and, therefore, can act as a coupling system to direct radiation into a waveguide. It means that such a modulated layer will support the excitation of standing waves. The narrow resonant features in Fig. 2 together with Fabry–Perot oscillations represent waveguides TE and TM modes of different orders, which are confirmed by the local electromagnetic fields distributions demonstrated in Fig. 3. The higher the surface grating amplitude, the more efficient the waveguide mode excitation. This is consistent with the spectral calculation results: the larger  $A$ , the deeper the dips in the spectrum corresponding to waveguide modes. Minor surface modulation inefficiently couples free space radiation into the waveguide mode, and the resonance Q factor is low (red curves (online) in Fig. 2). Theoretical estimations of the spectral position of standing modes can be made based on considerations of constructive interference:  $2nd = m\lambda$ . A shift in the mode position is observed with variation of the surface modulation amplitude, caused by an increase in the modulation  $A$ , a decrease in the thickness  $(d - A)$  of the parallel-sided plate, and the dependence of refractive index on the wavelength (see Fig. 2).

Figure 3 shows the distribution of local fields for the sample with the modulation of  $A = 20$  nm: magnetic field for TM polarization (Figs. 3a, 3b) and electric field for TE polarization (Figs. 3c, 3d). In the first case, the distributions are plotted for wavelengths of 801 and 897 nm. These positions are marked with black arrows in Fig. 2a. These are two subsequent modes, differing by one in the number of maxima—bright red spots inside the  $\text{As}_{50}\text{Se}_{50}$  layer along the position  $x = 0$ . A similar picture in the case of TE polarization is presented for wavelengths of 756 and

840 nm: these are two successive modes, differing by one in the number of maxima, the dips in the transmission spectrum for which are also marked with arrows in Fig. 2c. Moreover, in both cases the longer the wavelength, the smaller the mode number. The first, fundamental standing wave in the layer of such thickness will have a wavelength in the infrared region, which will correspond to the lowest frequency.

Complex transmittance and reflectance coefficients as functions of wavelength are obtained using the S-parameter calculation method. This approach allows one to extract the spectral dependence of the phase delay for both TE and TM polarizations sequentially. The difference between these two polarization phases determines the delay between the two basic components of the electric field, solving the problem of this study—extracting the polarization state after the interaction of light with a nanostructured medium. Figure 4 shows the spectral dependence of the phase difference calculated for several modulation amplitudes in the reflected geometry. The phase difference is zero for the unmodulated sample ( $A = 0$ , black curve), which confirms the validity of the approach, since any polarization, according to the Fresnel formulas, will yield the same result at normal incidence and in the absence of modulation. The phase delay increases and shifts spectrally following the position of the standing mode optical resonances when the modulation amplitude increases. This demonstrates the feasibility of designing nanostructured polarization compensators for different spectral ranges. The highest modulation is achieved for the sample with  $A = 100$  nm as follows from Fig. 4. The polarization state of the reflected light is further studied for this amplitude of the surface relief modulation (Fig. 5).

Next, the structure is illuminated with  $45^\circ$ -polarized light to the LIPSS grooves to demonstrate its suitability as a wave plate after understanding the basic polarizations. In this case, the delay between the electric field components along and across the grating is going to be maximized. This polarization corresponds to a linear combination of the basic vectors TE and TM. Fig. 5 demonstrates the light polarization states projected onto the  $x$ - and  $z$ -axes. The first panel shows that the incident wave polarization (black curve) is linear and oriented at  $\theta = 45^\circ$ —the  $E_x$  and  $E_z$  components have the same amplitude and zero phase delay, i.e., they are in phase. The red curve in Fig. 5a shows the polarization state of the reflected light for the structure without modulation. This is also a linear polarization, with a plane rotation angle of  $\theta = -45^\circ$ . This result is consistent with the known fact that, upon reflection from an optically denser medium, the wave phase changes by  $\pi$ . This result is satisfied for any wavelength, which is consistent with the data in Fig. 4, where there is no phase delay between the  $E_x$  and  $E_z$  components in the absence of surface modulation (black curve). Figures 5b–5d show the polarization



**Fig. 2.** Transmission (a, c) and reflectance (b, d) spectra of the sample illuminated with TM (a, b) and TE (c, d) polarization as a function of the surface modulation amplitude. Black curve: no modulation, red:  $A = 10$  nm, green:  $A = 20$  nm, blue:  $A = 50$  nm, cyan:  $A = 80$  nm, brown:  $A = 100$  nm. Colored arrow: guide to eye for spectrum shift with increasing amplitude. Inserts: enlarged spectral regions. Four black arrows show the wavelengths for which the field distribution is plotted.

state of the reflected light from the structure with a modulation of  $A = 100$  nm for three wavelengths—695, 783, and 869 nm. These positions are marked with gray dotted lines in Fig. 4. For a wavelength of 695 nm, the reflected light is elliptically polarized, the ratio of the ellipse semi-axes is  $15^\circ$ . In addition, a rotation of the plane of polarization occurs:  $\theta = 1^\circ$ . For a wavelength of 783 nm, there is almost no phase delay (ellipticity  $\varepsilon = 1^\circ$ ), and the rotation of the plane of polarization is also equal to  $1^\circ$ . Finally, for a wavelength of 869 nm, almost circular polarization is observed: ellipticity  $\varepsilon = 39^\circ$ , and the rotation of the plane of polarization  $\theta = -42^\circ$ .

The polarization plane rotation is caused by the different oscillation amplitudes of each field component according to the ellipse equation, which vary due to the different reflection coefficients of TE and TM waves at a fixed wavelength. Thus, for the wavelength of 869 nm, the reflectivity of TM ( $E_x$ ) polarized light is 31%, and TE ( $E_z$ ) is 30%, as follows from Figs. 2b and 2d, respectively. Therefore the amplitudes of the  $E_x$  and  $E_z$  components of the reflected field are close in values, which is confirmed by Fig. 5d. As follows from Fig. 4, the phase delay is close to  $\pi/2$ , therefore the reflected light is almost circularly polarized. For a wavelength of 783 nm, the reflectivity of TM waves is

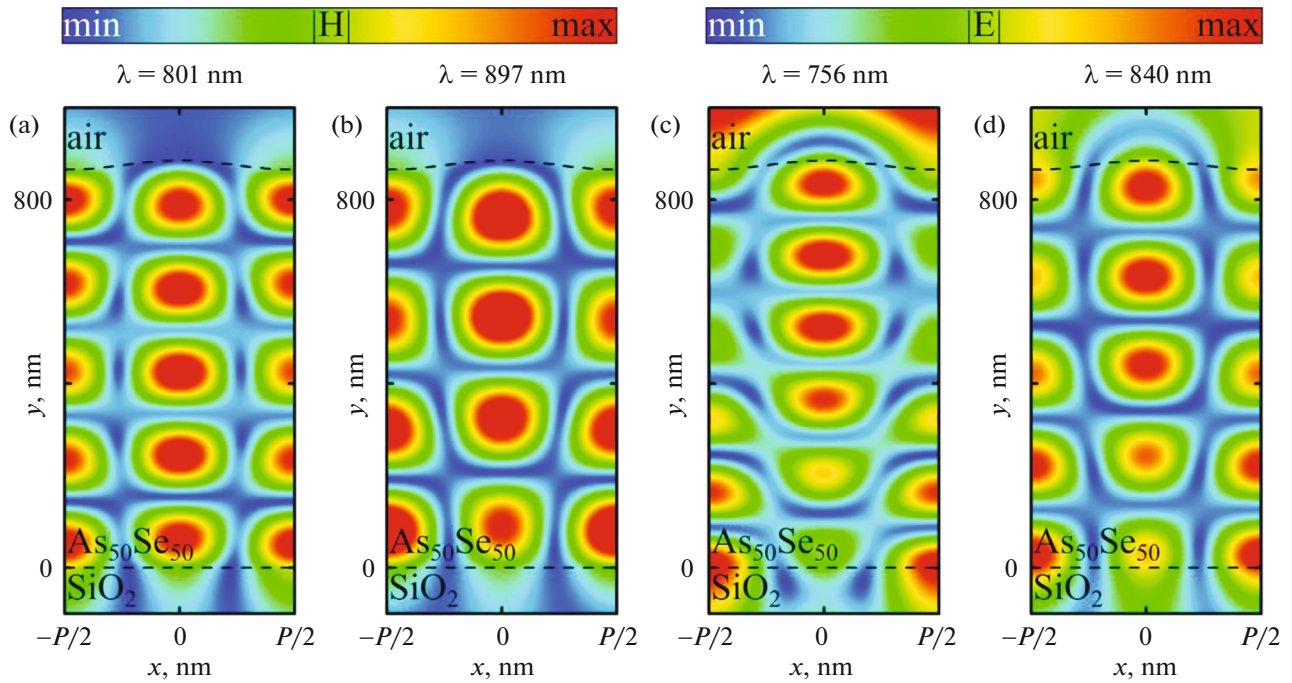


**Fig. 3.** Distribution of the local magnetic (a, b) and electric (c, d) fields for a modulation amplitude of  $A = 20$  nm, in the case of illumination with TM-polarized light for wavelengths of 801 and 897 nm (a, b) and TE-polarized light for wavelengths of 756 and 840 nm (c, d). Black dotted curves indicate the dimensions of the  $\text{As}_{50}\text{Se}_{50}$  layer.

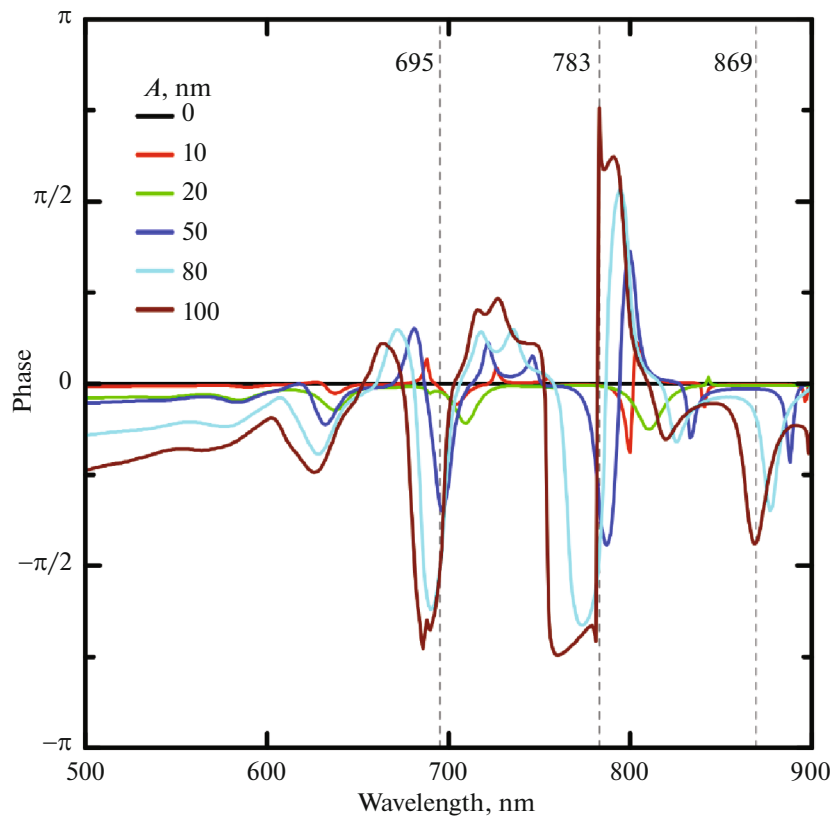


**Fig. 4.** Spectral dependence of the phase delay introduced by the sample. Black curve: no modulation, red:  $A = 10$  nm, green:  $A = 20$  nm, blue:  $A = 50$  nm, cyan:  $A = 80$  nm, brown:  $A = 100$  nm.

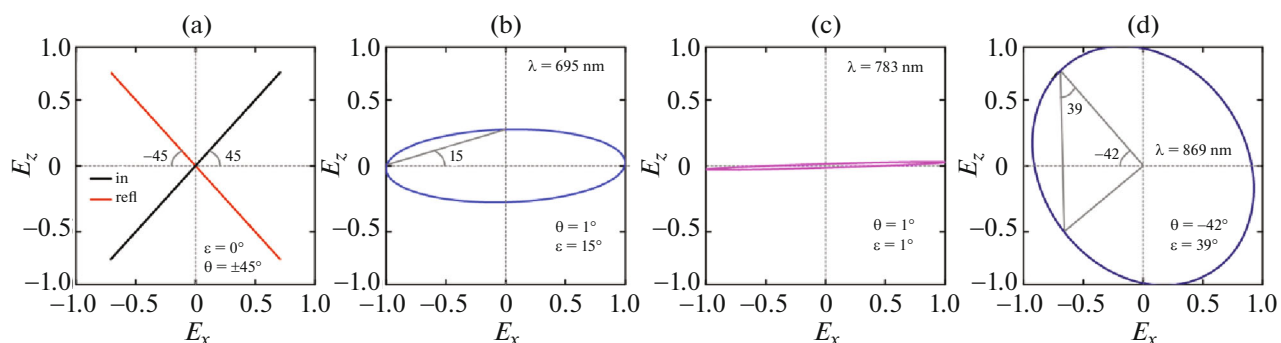


**Fig. 5.** Polarization states of incident light (a, black curve), reflected from the structure without modulation (a, red curve); reflected from the structure with modulation  $A = 100$  nm for wavelengths of 695 (b), 783 (c) and 869 nm (d).

80%, TE is 1% (Figs. 2b, 2d), therefore the  $Z$ -component field influence is insignificant, consequently, the light will be predominantly  $X$ -polarized, as can be seen in Fig. 5c. The polarization plane rotation of the reflected radiation relative to the  $X$ -axis is  $1^\circ$ , and the ellipticity is insignificant ( $1^\circ$ ). For a wavelength of 695 nm, the reflectivity TM is 36%, TE is 3%. Therefore, the reflected light is predominantly  $X$ -polarized as well, as shown in Fig. 5b, while the phase delay for this wavelength is  $85^\circ$  (Fig. 4).

The numerical simulations show that appropriate selection of nanostructure parameters allows one to obtain polarizing optical elements with the characteristics required by the user.

## CONCLUSIONS

Thus, this study numerically demonstrates the feasibility of using LIPSS deposited on  $\text{As}_{50}\text{Se}_{50}$  chalcogenide glasses as waveplates and polarization compensators. Direct writing of structured surfaces with proper LIPSS design can enable the formation of polarization elements with predetermined electromagnetic properties. The use of femtosecond laser irradiation to form a periodic surface relief is an example of promising top-to-bottom nanotechnology for functional optical elements fabrication, opening up new possibilities to create compact integrated photonic circuits.

## ACKNOWLEDGMENTS

The authors thank D.V. Pepeliaev.

## FUNDING

This work was supported by the Russian Science Foundation (grant no. 22-19-00035, <https://rscf.ru/project/22-19-00035>).

## CONFLICT OF INTEREST

The authors of this work declare that they have no conflicts of interest.

## REFERENCES

1. M. Born and E. Wolf, *Principles of Optics*, 7th ed. (Cambridge University Press, Cambridge, 1999; Nauka, 1973).
2. Z. Shen and X. Lin, *Opt. Mater.* **146**, 114567 (2023). <https://doi.org/10.1016/j.optmat.2023.114567>
3. Y. Hu, X. Wang, and X. Luo, *Nanophotonics* **9**, 3755 (2020). <https://doi.org/10.1515/nanoph-2020-0220>
4. S. Lei, X. Zhao, X. Yu, et al., *J. Manuf. Sci. Eng.* **142**, 031005 (2020). <https://doi.org/10.1115/1.4045969>
5. X. Wu, *Mater. Sci. Technol.* **23**, 631 (2007). <https://doi.org/10.1179/174328407X179593>
6. K. R. Safronov, V. O. Bessonov, D. V. Akhremenkov, et al., *Laser Photonics Rev.* **16**, 2100542 (2022). <https://doi.org/10.1002/lpor.202100542>
7. S. V. Zaboltnov, P. K. Kashkarov, A. V. Kolobov, and S. A. Kozyukhin, *Nanobiotechnol. Rep.* **18**, 829 (2023). <https://doi.org/10.1134/S2635167623600542>
8. A. Yu. Vorobyev and Ch. Guo, *Laser Photonics Rev.* **7**, 385 (2013). <https://doi.org/10.1002/lpor.201200017>
9. D. Shuleiko, S. Zaboltnov, O. Sokolovskaya, et al., *Materials* **16**, 4524 (2023). <https://doi.org/10.3390/ma16134524>
10. S. Höhm, M. Herzlieb, A. Rosenfeld, et al., *Appl. Surf. Sci.* **374**, 331 (2016). <https://doi.org/10.1016/j.apsusc.2015.12.129>
11. J. Li, J. Zhang, and C. Zhang, *Fund. Res.* (2025). <https://doi.org/>
12. A. San-Blas, M. Martinez-Calderon, J. Buencuerpo, et al., *Appl. Surf. Sci.* **520**, 146328 (2020). <https://doi.org/10.1016/j.apsusc.2020.146328>
13. D. Shuleiko, S. Zaboltnov, M. Martyshev, et al., *Materials* **15**, 7612 (2022). <https://doi.org/10.3390/ma15217612>

14. K. Bronnikov, S. Gladkikh, and E. Mitsai, *Opt. Laser Technol.* **169**, 110049 (2024).  
<https://doi.org/10.1016/j.optlastec.2023.110049>
15. Y. Shimotsuma, P. G. Kazansky, J. Qiu, et al., *Phys. Rev. Lett.* **91**, 5 (2003).  
<https://doi.org/10.1103/PhysRevLett.91.247405>
16. A. Zakery and S. R. Elliott, *J. Non-Cryst. Solids* **330**, 12 (2003).  
<https://doi.org/10.1016/j.jnoncrysol.2003.08.064>
17. T. Cardinal, K. A. Richardson, H. Shim, et al., *J. Non-Cryst. Solids* **256–257**, 353 (1999).  
[https://doi.org/10.1016/S0022-3093\(99\)00524-4](https://doi.org/10.1016/S0022-3093(99)00524-4)
18. S. Spalter, G. Lenz, R. E. Slusher, et al., *Optical Fiber Communication Conference. Technical Digest Post-conference Edition. Trends in Optics and Photonics*, Vol. 37 (IEEE Cat. No. 00CH37079) (2000).  
<https://doi.org/10.1109/OFC.2000.868545>
19. A. Feltz, *Amorphous and Glassy Inorganic Solids* (Wiley-VCH, 1993; Mir, Moscow, 1986).
20. E. Kuzmin, S. Zaboltnov, D. Shuleiko, et al., *Bull. Russ. Acad. Sci.: Phys* **88**, 370 (2024).  
<https://doi.org/10.1134/S106287382470984X>
21. J. B. Ramírez-Malo, C. Corrales, and E. Márquez, *Mater. Chem. Phys.* **40**, 30 (1995).  
[https://doi.org/10.1016/0254-0584\(94\)01451-L](https://doi.org/10.1016/0254-0584(94)01451-L)

**Publisher's Note.** Pleiades Publishing remains neutral with regard to jurisdictional claims in published maps and institutional affiliations. AI tools may have been used in the translation or editing of this article.